Astronomy & Astrophysics manuscript no.
(will be inserted by hand later)

Continuum Subtraction of the Discrete Source Foreground in EoR Observations

F. H. Briggs[1,2]⋆, A.G. de Bruyn[3,4]⋆⋆, M. van Haarlem[3]⋆⋆⋆

[1] RSAA, The Australian National University, Mount Stromlo Observatory, Cotter Road, ACT 2611, Australia
[2] ATNF, CSIRO, Epping, NSW, Australia
[3] ASTRON, Postbus 2, Dwingeloo, The Netherlands
[4] Kapteyn Institute, University of Groningen, Postbus 800, 9700 AV Groningen, The Netherlands

Received mmddyy/ accepted mmddyy

Abstract. Summary of Frank's continuum-subtraction calculations during his November 2003 visit to Dwingeloo and a compendium of plots on using quadratic fits to remove continuum in EoR observations.
Conclusion: Conventional methods of continuum subtraction in radio spectral line observations are more than adequate to suppress the signal of source clustering in the measurement of the redshifted 21cm line from evolving structure during the Epoch of Reionization.

Key words. Galaxies: formation: – radio lines – ISM – IGM – Epoch of Reionization

1. Variance from discrete source populations

The excitement surrounding the use of the 21cm line of hydrogen as a tomographic probe of growth of three dimensional structure during the epoch of reionization has awakened a concern about the contamination caused by discrete source foregrounds (Di Matteo et al. 2002, Mack & Oh 2002). Not only does (1) poisson noise in the source density cause variance in the radio continuum from pixel to pixel in the sky, but so also does (2) large scale structure, as quantified by the angular correlation function. A further complication in removal of the continuum is (3) the broad distribution of source spectral indices, which cause a variable curvature in the integrated spectra each resolution element in the sky.

Here, we show that standard radio astronomical continuum-subtraction methods are adequate for subracting the discrete source contamination on a pixel by pixel basis. These methods succeed in reducing the discrete source and clustering noise to a level below the expected EOR signal.

2. Method of analysis

Monte Carlo simulations are an effective way to appraise the contamination from the discrete discrete source population and the ability of continuum subtraction methods at reducing the added variance. The method is outlined as follows:

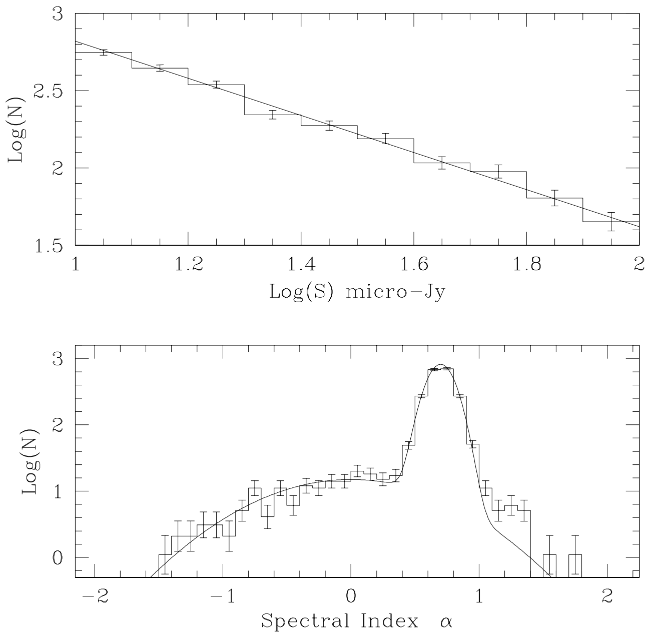

Fig. 1. Distribution of randomly drawn sample of radio sources in one $10' \times 10'$ pixel. Upper panel: distribution of 150 MHz flux densities in the range 10 to 100 μJy. Lower panel: distribution of spectral index. Histograms present one randomized realization of the source catalog for one pixel. Solid curves represent the parent distribution functions.

1. We randomly generate a catalog of discrete sources using the expression for source counts at faint levels given by Subrahmanyan (2002):

$$n(S)\,ds = 10^2\,S_{\mu Jy}^{-2.2}\,f_{GHz}^{-0.8}\,dS_{\mu Jy}\ \mathrm{arcmin}^{-2} \qquad (1)$$

Send offprint requests to: XXX
⋆ fbriggs@mso.anu.edu.au
⋆⋆ bruyn@astron.nl
⋆⋆⋆ haarlem@astron.nl

This formuation agrees within a factor ∼2 of other measures of the faint source counts and with our own experiences at Westerbork.
2. A typical catalog has 1000 pixels, and each pixel is square, with dimensions ranging from 1′ to 20′ on a side.
3. The fluctuation in flux density per pixel is dominated by the random occurences of the brightest sources in the sum, so our simulation adopts the common observational practice of applying "source subtraction", whereby all the sources brighter than a cut off level S_{cut} are identified in the dataset by high resolution imaging and their continuum contribution subtracted. This process leaves behind sources with flux density less than S_{cut}; among these sources, it is those at the bright limit of the sample that dominate the fluctuations. Therefore the simulation builds catalogs from a lower limit in flux density, S_0, to S_{cut}. For the majority of the catalogs, these values are $S_0 = 10\ \mu$Jy and $S_{cut} = 100\ \mu$Jy. Fig. 1 shows a sample of the flux density distribution for one pixel with these limits.
4. The mean number of sources per pixel $< N_s >$ is specified by eqn. 1 providing an average source density of ∼22 sources per arcmin^2 for catalogs of source with flux densities in the range 10 to 100 μJy. With the invocation of Poisson statistics, the number per pixel varied randomly with variance $< N_s >$ about the mean.
5. The majority of the source catalogs were generated at 150 MHz. Each source is also randomly assigned a spectral index α ($S \propto f^{-\alpha}$) in order to compute a realistic spectrum for each pixel from the sum of the flux densities of the radio sources in that pixel. The spectral index distribution has two components: 90% of the sources are drawn from a Gaussian distribution with $\sigma_\alpha = 0.1$ centered on $\alpha = 0.7$, and the other 10% from a distribution with $\sigma_\alpha = 0.6$ centered on $\alpha = 0$. Fig. 1 shows an example distribution for one pixel.
6. The catalogs are analyzed in the manner of radio astronomical spectral line datacubes of 1000 pixels after the integral spectrum for each pixel has been generated as described above (see Fig. 3). Since these simulations are modeling observations to be made with interferometer arrays, there will be no "zero spacing" flux densities available, and this means that the average flux density per frequency plane of the datacube will be constrained at zero. Thus, in the simulation, we compute the average flux density for each plane of the cube and then subtract that average from each pixel in that plane. This leaves behind the residual fluctuations from the discrete source foreground that an interferometer array would sense.
7. Large scale structure or clustering of the disrcete sources adds an additional variance to the number of sources per pixel, and this couples more variance to each plane in the datacube. These simulations include the additional variance using the formulation of Blake and Wall (2002): The Blake-Wall angular correlation function is $w(\theta) = 10^{-3}\theta^{-0.8}$ for θ measured in degrees. The net variance in the number of sources per pixel has contributions from both Poisson statistics and large scale structure. The net variance is $\mu_2 =< N_s > (1 + y < N_s >)$, where the y parameter results from an integral of the form:

$$< y >= \int w(\theta)\frac{dG_p}{d\theta}d\theta \qquad (2)$$

For the Blake-Wall parameters, this reduces to $< y >= 2\ 10^{-3}L^{-0.8}I$ where L is the dimension of the square pixel in degrees and $I = 1.12$ is the integral of the expression plotted in Fig. 4.
8. The simulations handle the continuum subtraction in the manner practiced by radio astronomers making spectral

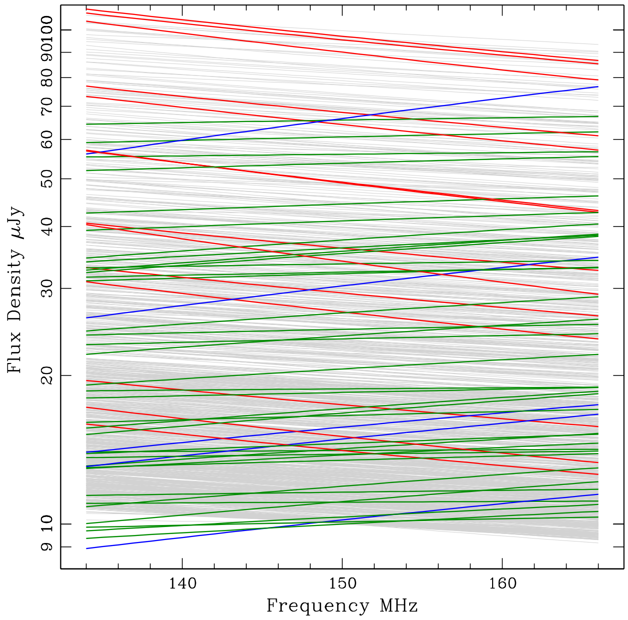

Fig. 2. Spectra for the random population of sources in one 10′×10′ pixel. Colored spectra are extra-steep and inverted spectra, while gray spectra are α = 0 to 1 ($S_\nu \propto \nu^{-\alpha}$).

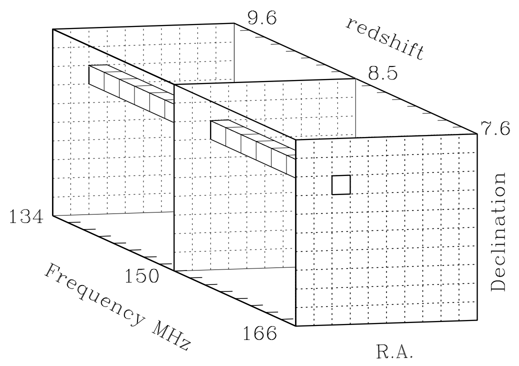

Fig. 3. Spectral line data cube. The spectral information for one R.A, Declination coordinate has been drawn in for emphasis. Since radio interferometers do not measure the 'zero spacing flux density,' the average flux density of each frequency plane of the cube is equal to zero. Spectral baseline removal fitting the residual continuum for each R.A-Dec pixel separately with a polynomial. The fitted function is then subtracted from the values as a function of frequency.

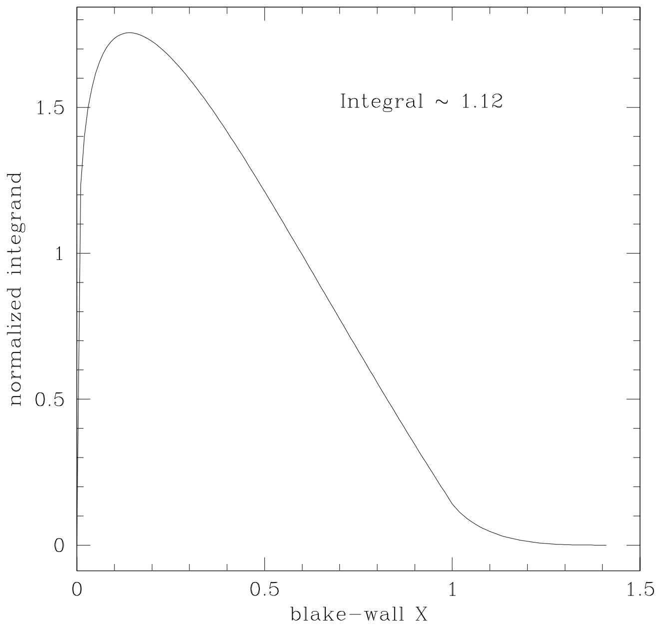

Fig. 4. The integrand of the Blake-Wall (2002) special function integral Eq. 2 for square areas, such as our model's pixels. The Blake-Wall $X = \theta/L$ where L is the length of the side of the square pixel whose source population we are summing. The value of the normalized integral is 1.12.

line observations. The brightest discrete source are subtracted by identifying their position and flux density as a function of frequency. In our simulations, we begin at the stage where the bright sources have been subtracted to a level of S_{cut}. The remaining flux density is subtracted using spectral fits to each pixel in the datacube (see Fig. 3). For each RA-dec pixel in the cube, we extract the spectrum and perform both linear and quadratic fits to the flux densities. For appraisal of the level of success at removing the fluctuation imposed by the discrete source population, we measure the *rms* fluctuation in each frequency plane of the cube after the linear and quadratic fits have been subtracted. These residual variances are plotted in the Figs. 5-14 as a function of frequency.

3. Discussion

The general result is that the conventional pixel by pixel continuum subtracton brings the fluctuation due to discrete source populations to a level below that of the expected 21cm line signal from the epoch of reionization. Under some circumstances, the linear fits are adequate, but more generally, a quadratic fit is necessary.

3.1. Variance as function of Pixel Size

Figures 5-10 illustrate the residual variance as a function of pixel size for 1′, 3′, 10′, and 20′ arcminute square pixels. The figures give (1) integral flux density as a function of frequency for source in the range 10μJy to 100μJy at 150 MHz, (2) the rms fluctuation in each frequency plane prior to function fitting and subtraction, (3) the rms fluctuation after subtracting linear spectral fits on a pixel by pixel basis, and (4) the rms fluctuation after subtraction of quadratic fits. The discrete source variances were computed and plotted for purely Poisson statistics and Poisson plus clustering. The residual rms levels in flux density are also transformed to rms brightness temperature fluctuations for pixels with these dimensions, so that they can be compared to the nominal rms brightness temperature signal strengths expected to appear in the 21cm line during the epoch of reionization.

Figures 9 and 10 compare the rms fluctuations for different pixel sizes for the pure Poisson case and Poisson plus clustering cases, respectively.

3.2. Variance as a function of bright source cut off S_{cut}

Figure 11 illustrates the dependency of the bright source cut off for S_{cut} taking the values 0.1 mJy, 0.3 mJy, 1 mJy, and 3 mJy. These calculations assume 10′ pixels and include clustering statistics.

3.3. Variance as a function of band center frequency

Since source strengths for the discrete source population rises significantly toward lower frequencies, we consider three settings for the center of the observing band: 100, 150 and 200 MHz, corresponding to redshifted HI at z = 13.2, 9.5 and 6.1. (See figs 12 to 14.) Again, these calculations are for 10′×10′ pixels, S_0 =10μJy and S_{cut} =300μJy.

Acknowledgements. The authors are grateful...

References

Blake, C., Wall, J. 2002, MNRAS, 337, 993
Di Matteo, T., Perna, R., Abel, T., Rees, M.J. 2002, ApJ, 564, 576
Oh, S.P., Mack, K.J. 2002, subm to MNRAS, astro-ph/0302099
Subrahmanyan, R. 2002, in The Universe at Low Radio Frequencies, IAU Symp, Vol 199, eds. A.P. Rao, G. Swarup and Gopal-Krishna, p. 58.

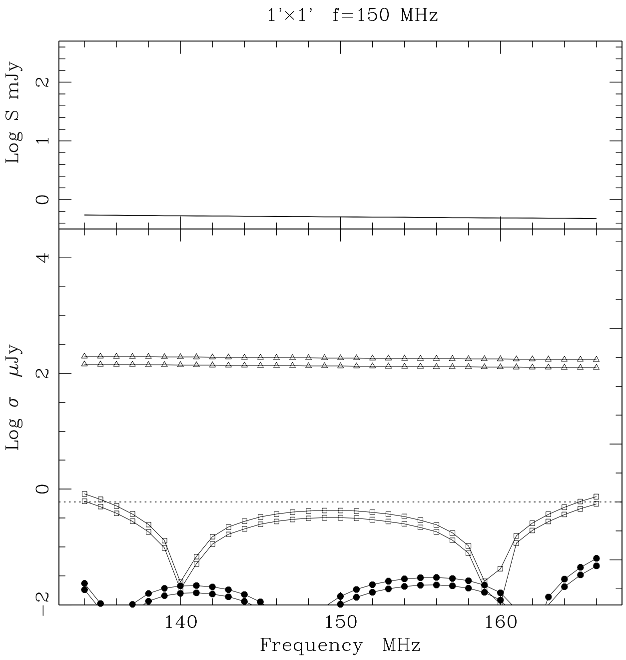

Fig. 5. Comparison of pure poisson and clustered distributions for 1′×1′ pixels. Top panel: integral flux density vs. frequency. Bottom panel: Open triangles are *rms* deviations without continuum subtraction. Open squares are rms residuals linear spectral baseline subtraction. Filled circles are rms residuals after quadratic baseline subtraction. Upper curve in each case includes galaxy correlation function fluctuations, while the lower curve is pure poisson statistical fluctuation based on mean source count statistics. Horizontal dotted line marks the 10 mK level, which is typical of the *rms* fluctuations expected for the EoR signal. The righthand axis indicates $\log T_B$ for this pixel size.

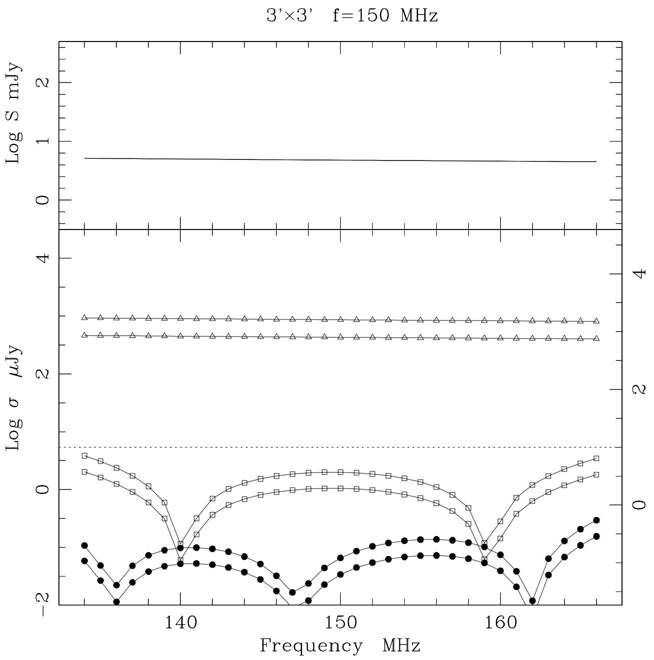

Fig. 6. Comparison of pure poisson and clustered distributions for 3′×3′ pixels as for Fig. 5.

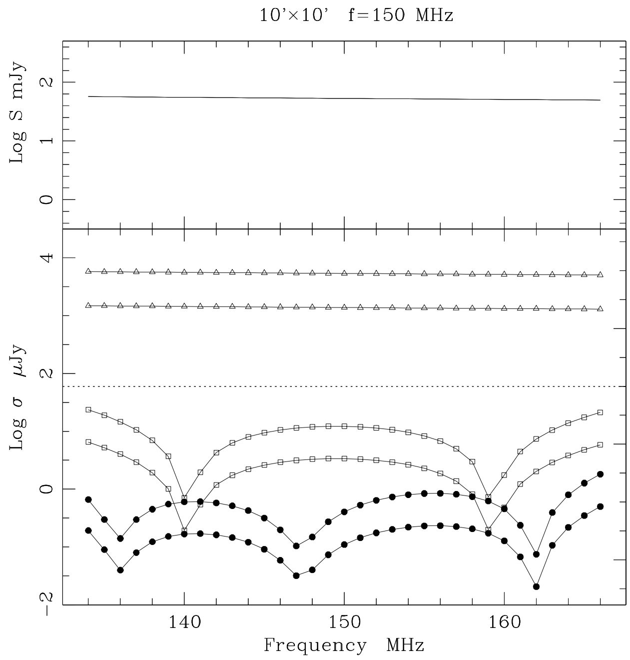

Fig. 7. Comparison of pure poisson and clustered distributions for 10′×10′ pixels as for Fig. 5.

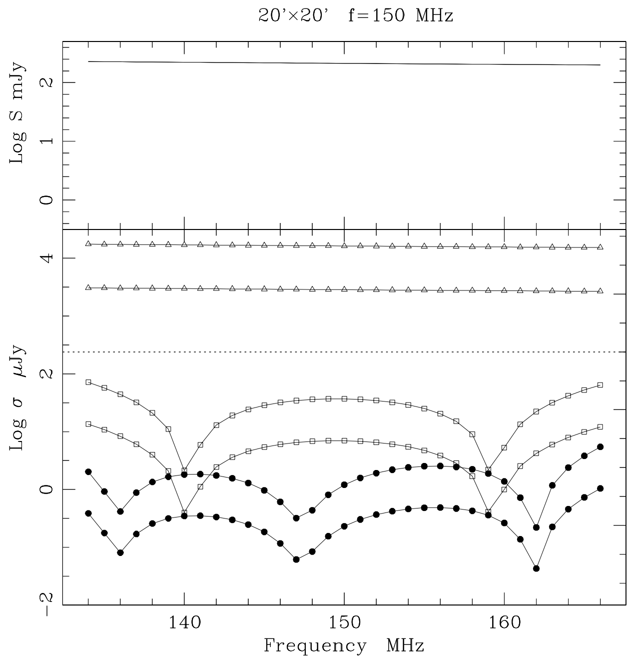

Fig. 8. Comparison of pure poisson and clustered distributions for 20′×20′ pixels as for Fig. 5.

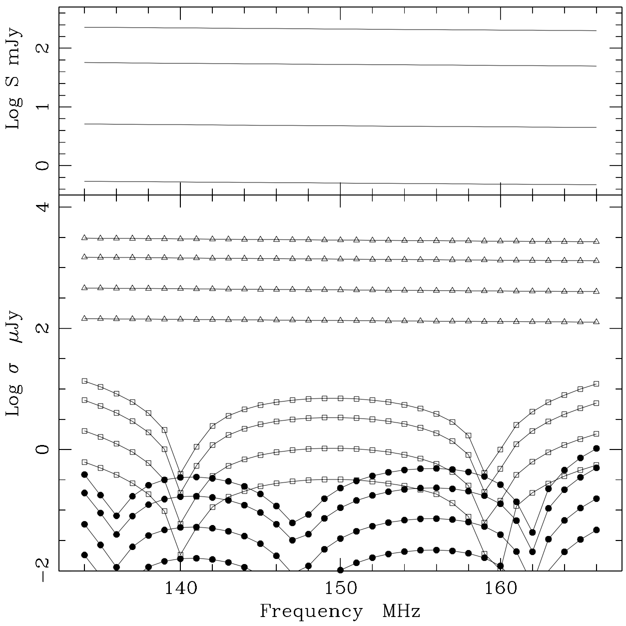

Fig. 9. Comparison fluctuation levels for 1′, 3′, 10′, and 20′ square pixels for Poisson statistical variations in source sky density. Top panel: integral flux density vs. frequency. Bottom panel: Open triangles are *rms* deviations without continuum subtraction. Open squares are rms residuals linear spectral baseline subtraction. Filled circles are rms residuals after quadratic baseline subtraction. The range from lowest to top curve for each case indicates increasing pixel size.

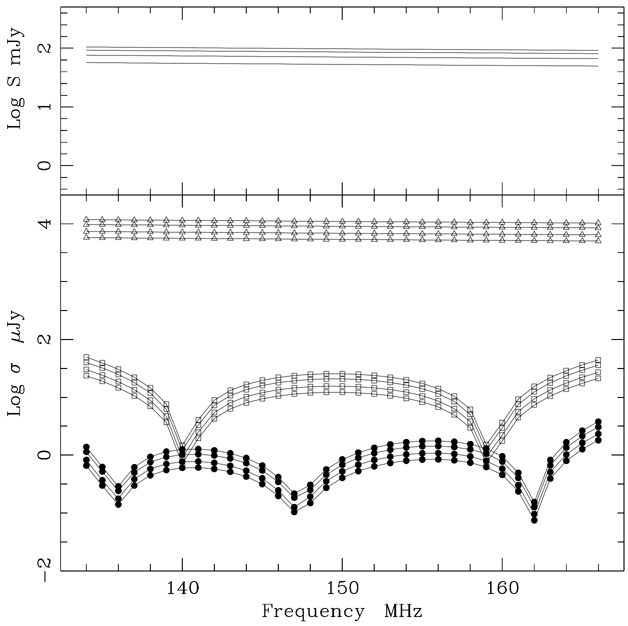

Fig. 11. Comparison fluctuation levels at different continuum cut-levels: S_{cut} = 0.1, 0.3, 1 and 3 mJy. These models are for 10′×10′ square pixels and include galaxy clustering in the statistical variations in source sky density. The models include a distribution of sources of flux density froim 10 μJy and S_{cut}. Curves are marked as indicated for Fig. 9.

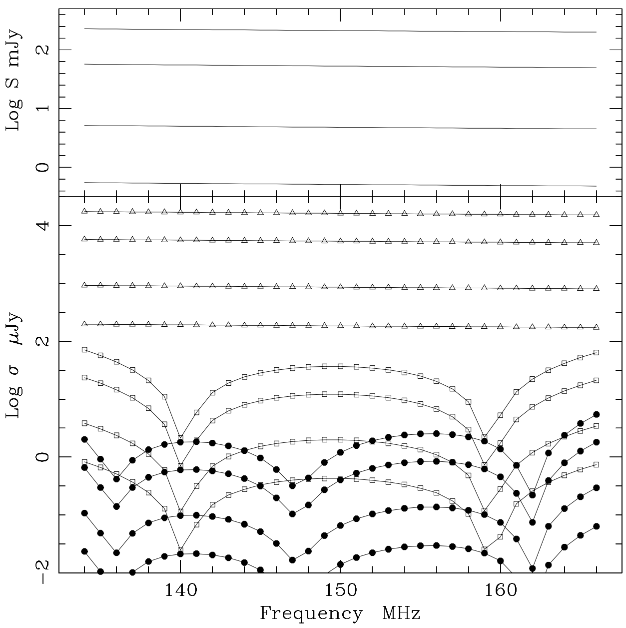

Fig. 10. Comparison fluctuation levels for 1′, 3′, 10′, and 20′ square pixels when galaxy clustering is added to the statistical variations in source sky density. Curves are marked as indicated for Fig. 9.

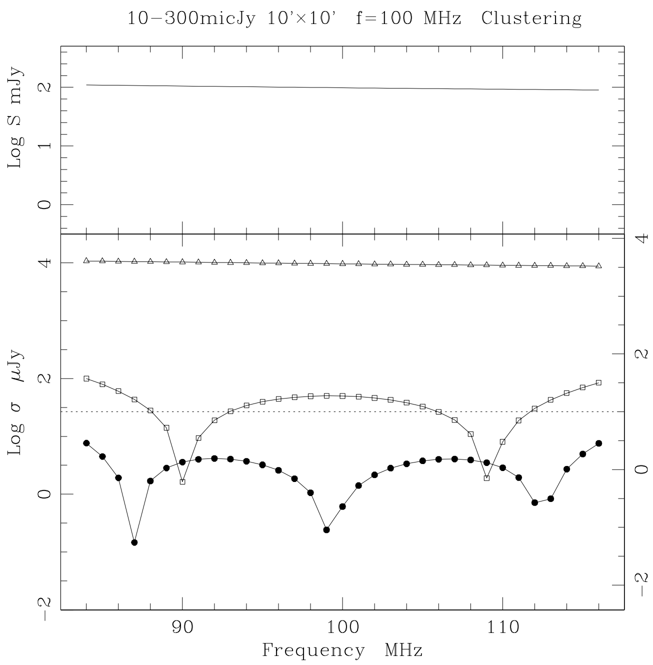

Fig. 12. Fluctuation levels at 100 MHz for models of 10′×10′ square pixels, including galaxy clustering in the statistical variations in source sky density. Top panel: Continuum flux density. Bottom panel: Open triangles are *rms* deviations without continuum subtraction. Open squares are rms residuals linear spectral baseline subtraction. Filled circles are rms residuals after quadratic baseline subtraction. $\log T_B$ mK is marked on the righthand side.

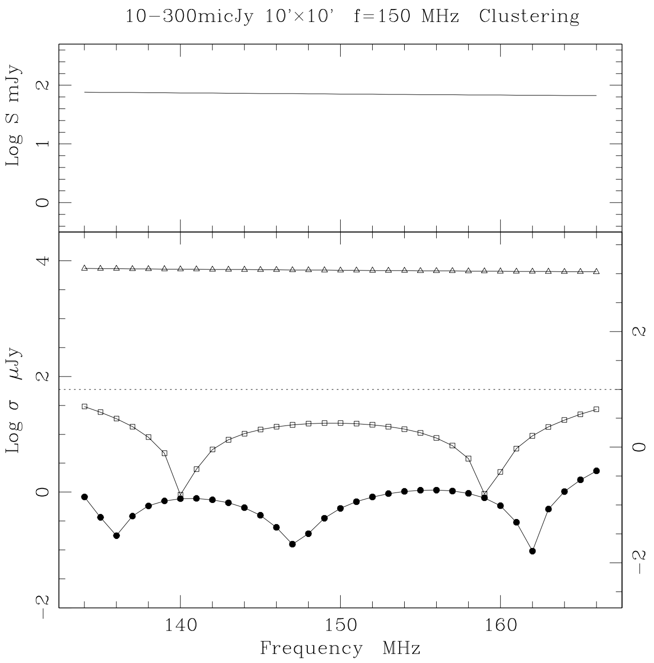

Fig. 13. Fluctuation levels at 150 MHz for models of $10' \times 10'$ square pixels, including galaxy clustering in the statistical variations in source sky density. Symbols are as in Fig. 12

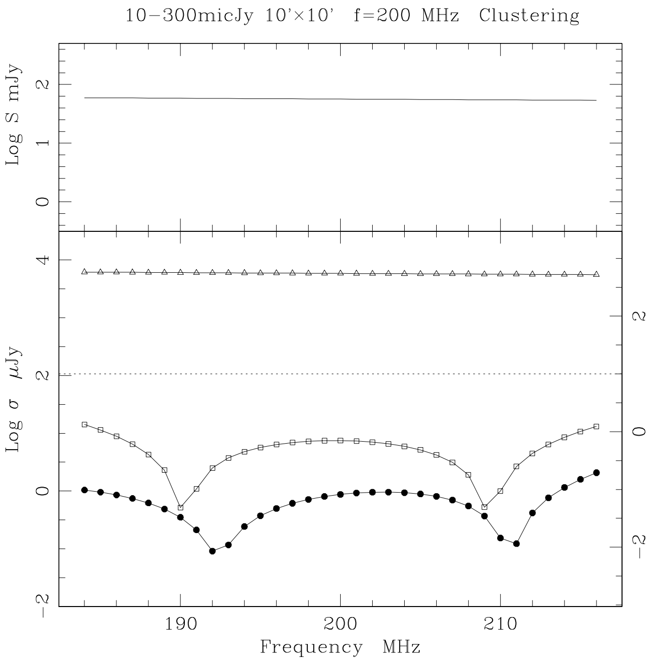

Fig. 14. Fluctuation levels at 200 MHz for models of $10' \times 10'$ square pixels, including galaxy clustering in the statistical variations in source sky density. Symbols are as in Fig. 12